Journal of Computational Physics **165,** 167–188 (2000)
doi:10.1006/jcph.2000.6609, available online at http://www.idealibrary.com on IDEAL®

A Projection FEM for Variable Density Incompressible Flows

J.-L. Guermond* and L. Quartapelle†

**Laboratoire d'Informatique pour la Mécanique et les Sciences de l'Ingénieur, CNRS, B.P. 133, 91403, Orsay, France; and †Dipartimento di Ingegneria Aerospaziale, Politecnico di Milano, Via La Masa 34, 20158 Milan, Italy*
E-mail: guermond@limsi.fr

Received October 5, 1999; revised March 13, 2000; published online November 3, 2000

This work describes a new finite element projection method for the computation of incompressible viscous flows of nonuniform density. One original idea of the proposed method consists in factorizing the density variable *partly outside and partly inside* the time evolution operator in the momentum equation, to prevent spatial discretization errors in the mass conservation to affect the kinetic energy balance of the fluid. It is shown that unconditional stability in the incremental version of the projection method is possible provided two projections are performed per time step. In particular, a second order accurate BDF projection method is presented and its numerical performance is illustrated by test computations and comparisons. © 2000 Academic Press

Key Words: variable density Navier–Stokes equations; incompressible flows of nonuniform density; fractional step projection method; poisson pressure equation; incremental second order projection method; BDF scheme; finite elements; mixed method.

1. INTRODUCTION

Simulating variable density incompressible flows presents the difficulty of satisfying the property of mass conservation twice. On one hand, the mass density of each fluid particle must remain unchanged during the fluid motion, whatever the level of unsteadiness and mixing. On the other hand, the velocity field must satisfy the incompressibility constraint, which reflects the unability of pressure to do compression work. These two important physical characteristics are fully described by the set of incompressible Navier–Stokes equations augmented by the advection equation for the density. For the mathematical theory of existence and uniqueness of solutions to this set of equations, we refer to Lions [10]. This theory is far from trivial, because the equations governing the motion of a

0021-9991/00 $35.00

variable density but incompressible fluid constitute a mixed PDE system entangling hyperbolic, parabolic, and elliptic features. Variable density incompressible Navier–Stokes equations are important in several fields of fluid dynamics: for instance, in highly stratified flows, in the study of the dynamics of interfaces between fluid of different density, and in problems of inertial confinement and problems of astropysics.

For developing numerical approximations to this problem, it seems natural to exploit, as far as possible, the techniques established for the solution of constant density incompressible Navier–Stokes equations, viz., the fractional step projection method of Chorin [2, 3] and Teman [13, 14]. For instance, this approach has been followed by Bell and Marcus [1], who proposed a solution method based on finite differences.

Since in the past few years we have developed a finite element projection method of incremental type of second-order time accuracy [7, 9], we have attempted to extend its application to variable density problems. In this paper we report on how such an extension has been accomplished without sacrificing any of the distinctive features of the method we started from, namely, unconditional stability, $\mathcal{O}(h^3)$ spatial accuracy, and $\mathcal{O}(\Delta t^2)$ accuracy in time. Let us now comment briefly on these characteristics, separately.

As far as the stability is concerned, the main issue is to ensure *a priori* that the spatial discretization errors associated with the approximate fulfillment of mass conservation does not affect the balance of kinetic energy. Nonlinear instability can be avoided provided the particle derivative of momentum is written in a way that accounts for density variations without invoking mass conservation to guarantee the energy balance. This requires writing the density variable ρ in the evolutionary term of the momentum equation as the product of two $\sqrt{\rho}$, one occurring outside and the other inside the time derivative operator. Realizing that this form is suitable for not affecting the energy balance is possible by looking at the problem within a variational formulation.

Concerning the issue of the spatial accuracy, we propose a mixed finite element technique where the density and the velocity are approximated in the same space. This choice makes it very easy to develop the new method from an existing FEM solver dedicated to the solution of uniform density flows. In our implementation, we use the $\mathbb{P}_1$–$\mathbb{P}_2$ interpolation.

Finally, about temporal accuracy, we use an incremental fractional step technique based on the second order accurate BDF scheme. By analyzing the stability of the method in a way similar to that in [5], we find that, to preserve the unconditional stability in the variable density problem, two projection steps per time step are needed. The first projection must be performed after the time advancement of the mass conservation equation but before that of the momentum equation. The variable coefficient elliptic operator of the first, preliminary projection is found to coincide with that of the second, standard projection step.

The paper is organized as follows. In Section 2 we review the governing equations and reformulate them so that the kinetic energy balance is fully uncoupled from the mass conservation. In Section 3 an unconditionally stable nonincremental projection method for variable density problems is built. This step sets all the tools that are necessary for developing the incremental version of the projection method. In Section 4 we build the incremental method and show that it is unconditionally stable provided that an auxiliary pressure unknown is introduced and two projections are performed per time step. Section 5 details the introduction of a three-level BDF time stepping for reaching second order accuracy in time and gives the complete set of equations defining the proposed algorithm. In Section 6 the error estimates of the method are verified by solving a simple analytical problem; two test

problems of Rayleigh–Taylor instability are finally considered. The last section is devoted to concluding remarks.

2. GOVERNING EQUATIONS

We are hereafter concerned with the time-dependent Navier–Stokes equations for a fluid whose density may vary both in space and time but which is nevertheless incompressible, in the sense that each fluid particle retains its initial density during the entire subsequent motion. In the following, the fluid domain Ω is assumed to be smooth, bounded, and connected in two or three dimensions.

2.1. *Variable Density Navier–Stokes Equations*

The equations governing the flows of interest comprise the continuity equation expressing the mass conservation, the momentum equation accounting for the Newton second law, and the kinematic constraint of solenoidality for the velocity field. These equations are expressed in terms of the primitive variables: density ρ, velocity $\boldsymbol{u}$, and pressure P. The mathematical statement of the problem is: Find $\rho > 0, \boldsymbol{u}$, and P up to a constant (actually, up to an arbitrary function of t only) so that

$$\begin{cases} \frac{\partial \rho}{\partial t} + \boldsymbol{\nabla} \cdot (\rho \boldsymbol{u}) = 0, \\ \frac{\partial (\rho \boldsymbol{u})}{\partial t} + \boldsymbol{\nabla} \cdot (\rho \boldsymbol{u} \otimes \boldsymbol{u}) - \mu \nabla^2 \boldsymbol{u} + \boldsymbol{\nabla} P = \boldsymbol{f}, \\ \boldsymbol{\nabla} \cdot \boldsymbol{u} = 0, \end{cases} \tag{2.1}$$

where $\mu > 0$ the (shear) viscosity of the fluid (assumed here to be a constant) and $\boldsymbol{f}$ is a known body force (per unit volume), possibly dependent on space, time, or both; typically, in stratified flows, $\boldsymbol{f} = \rho \boldsymbol{g}$, $\boldsymbol{g}$ being the gravity field. We recall that $\boldsymbol{\nabla} \cdot (\rho \boldsymbol{u} \otimes \boldsymbol{u}) = \partial_j (\rho u_i u_j) = u_j \partial_j (\rho u_i) + \rho u_i \partial_j u_j = (\boldsymbol{u} \cdot \boldsymbol{\nabla})(\rho \boldsymbol{u}) + \rho \boldsymbol{u} \boldsymbol{\nabla} \cdot \boldsymbol{u}$. The viscous stress contribution resulting from bulk viscosity is zero by the assumed incompressibility of the flow.

The complete mathematical statement of the problem requires suitable boundary and initial conditions which read

$$\begin{aligned} \rho|_{\Gamma_{\text{in}}} &= a, \quad \rho|_{t=0} = \rho_0, \\ \boldsymbol{u}|_{\Gamma} &= \boldsymbol{b}, \quad \boldsymbol{u}|_{t=0} = \boldsymbol{u}_0, \end{aligned} \tag{2.2}$$

where $a > 0$ and $\boldsymbol{b}$ are respectively the density and velocity prescribed on the boundary, whereas $\rho_0 > 0$ and $\boldsymbol{u}_0$ are the initial distribution of density and velocity. In accordance with the hyperbolic character of the mass conservation equation, the portion Γ_{in} of the boundary where the density is specified is defined by

$$\Gamma_{\text{in}} \equiv \{\boldsymbol{r} \in \Gamma \mid \boldsymbol{n} \cdot \boldsymbol{b}(\boldsymbol{r}) < 0\}, \tag{2.3}$$

where $\boldsymbol{n}$ is the outward unit normal to the boundary Γ. Γ_{in} can in general depend on time, namely, $\Gamma_{\text{in}} = \Gamma_{\text{in}}(t)$, because of a possible variation in time of the velocity boundary datum, $\boldsymbol{b} = \boldsymbol{b}(t)$. It must be stressed that, exactly as in the Navier–Stokes problem for a homogeneous fluid, neither a boundary condition nor an initial condition is required for the pressure.

For the sake of simplicity, only a Dirichlet boundary condition for velocity is considered here, but more general boundary conditions can be handled by the techniques presented below. In particular, it is worth noticing that, for a homogeneous Dirichlet condition on the normal component of the velocity on the entire Γ, no boundary condition needs to be specified for the density.

The solvability of the problem defined by the equation system (2.1) supplemented with the boundary and initial conditions (2.2) requires the satisfaction of the conditions on the boundary and initial data for the velocity

$$\int_\Gamma \boldsymbol{n} \cdot \boldsymbol{b} = 0, \quad \forall t \geq 0, \quad \text{and} \quad \boldsymbol{\nabla} \cdot \boldsymbol{u}_0 = 0, \tag{2.4}$$

as well as the fulfillment of a compatibility condition between these two data,

$$\boldsymbol{n} \cdot \boldsymbol{b}|_{t=0} = \boldsymbol{n} \cdot \boldsymbol{u}_0|_\Gamma. \tag{2.5}$$

2.2. *Stability of the Equation System*

In the formulation that we propose, the mass conservation and momentum equations are recast in a form that guarantees some control on the L^2-norm of the density and on the kinetic energy of the fluid.

First, we observe that the theory of characteristics applied to the mass conservation equation under the incompressibility assumption, namely,

$$\frac{\partial \rho}{\partial t} + \boldsymbol{u} \cdot \boldsymbol{\nabla} \rho = 0,$$

implies that, if $\rho_0(\boldsymbol{r})$ is such that $0 < \alpha \leq \rho_0(\boldsymbol{r}) \leq \beta, \forall \boldsymbol{r} \in \Omega$, then it holds that $0 < \alpha \leq \rho(\boldsymbol{r}, t) \leq \beta$ for any $t > 0$. Moreover, multiplying the mass transport equation above by ρ and integrating over Ω, we obtain

$$\int_\Omega \rho \frac{\partial \rho}{\partial t} + \int_\Omega \rho \boldsymbol{u} \cdot \boldsymbol{\nabla} \rho = \frac{d}{dt} \frac{1}{2} \int_\Omega \rho^2 = 0,$$

since $\int_\Omega \rho \boldsymbol{u} \cdot \boldsymbol{\nabla} \rho = \frac{1}{2} \int_\Omega \boldsymbol{u} \cdot \boldsymbol{\nabla}(\rho^2) = 0$ by integration by parts, thanks to the flow incompressibility and the boundary condition for the normal component of velocity, which is assumed here and in the following to be homogeneous, namely, $\boldsymbol{n} \cdot \boldsymbol{u}|_\Gamma = 0$. As a result we have

$$\|\rho(\cdot, t)\|_0 = \|\rho_0\|_0, \tag{2.6}$$

where $\|\cdot\|_0$ denotes the L^2 norm of functions defined in Ω. Note that we needed to invoke incompressibility to derive this identity. As a result, this property will be lost at the discrete level because the incompressibility constraint will be enforced weakly only. To avoid this difficulty, we rewrite the nonlinear term $\boldsymbol{u} \cdot \boldsymbol{\nabla} \rho$ in the mass conservation equation in its skew symmetric form $\boldsymbol{u} \cdot \boldsymbol{\nabla} \rho + \rho \boldsymbol{\nabla} \cdot \boldsymbol{u}/2$:

$$\frac{\partial \rho}{\partial t} + \boldsymbol{u} \cdot \boldsymbol{\nabla} \rho + \frac{\rho}{2} \boldsymbol{\nabla} \cdot \boldsymbol{u} = 0. \tag{2.7}$$

Owing to Lemma 1, it can be verified that this form of the mass conservation equation guarantees that the L^2 norm of ρ is constant in time without invoking incompressibility. As a result, this property will be preserved at the discrete level.

LEMMA 1. *For φ and $\boldsymbol{v}$ regular enough and $\boldsymbol{v}$ such that $\boldsymbol{n}\cdot\boldsymbol{v}|_\Gamma = 0$ we have*

$$\int_\Omega \left[\varphi \boldsymbol{v}\cdot\boldsymbol{\nabla}\varphi + \frac{1}{2}\varphi^2 \boldsymbol{\nabla}\cdot\boldsymbol{v}\right] = 0.$$

Coming now to the momentum equation, let us assume, for the sake of simplicity of the argument, that $\boldsymbol{f} = 0$. Multiplying the momentum equation by $\boldsymbol{u}$ yields

$$\int_\Omega \boldsymbol{u}\cdot\frac{\partial(\rho u)}{\partial t} + \int_\Omega \boldsymbol{u}\cdot[\boldsymbol{\nabla}\cdot(\rho\boldsymbol{u}\otimes\boldsymbol{u})] + \mu\int_\Omega |\boldsymbol{\nabla}\boldsymbol{u}|^2 = 0,$$

where we have used integration by parts and $\boldsymbol{u}|_\Gamma = 0$. The pressure term has disappeared because $\int_\Omega \boldsymbol{u}\cdot\boldsymbol{\nabla}P = 0$ by virtue of $\boldsymbol{\nabla}\cdot\boldsymbol{u} = 0$ and of $\boldsymbol{n}\cdot\boldsymbol{u}|_\Gamma = 0$. The first two terms can be handled by means of the identity

$$\boldsymbol{u}\cdot\left[\frac{\partial(\rho\boldsymbol{u})}{\partial t} + \boldsymbol{\nabla}\cdot(\rho\boldsymbol{u}\otimes\boldsymbol{u})\right] = \frac{1}{2}\left[\frac{\partial(\rho|\boldsymbol{u}|^2)}{\partial t} + \boldsymbol{\nabla}\cdot(\rho|\boldsymbol{u}|^2\boldsymbol{u})\right],$$

which is obtained by using the rule for the derivative of products (twice) and the mass conservation equation (once). By means of this identity and using again $\boldsymbol{\nabla}\cdot\boldsymbol{u} = 0$ and $\boldsymbol{n}\cdot\boldsymbol{u}|_\Gamma = 0$, we infer

$$\frac{d}{dt}\int_\Omega \rho|\boldsymbol{u}|^2 + 2\mu\int_\Omega |\boldsymbol{\nabla}\boldsymbol{u}|^2 = 0,$$

from which we deduce immediately that $\int_\Omega(\rho|\boldsymbol{u}|^2)(\boldsymbol{r},t) \le \int_\Omega \rho_0|\boldsymbol{u}_0|^2$, an inequality that can be expressed in the form

$$\|(\sqrt{\rho}\boldsymbol{u})(\cdot,t)\|_0 \le \|\sqrt{\rho_0}\boldsymbol{u}_0\|_0, \tag{2.8}$$

$\|\cdot\|_0$ denoting also the L^2 norm of vector functions. Note that $\|\sqrt{\rho}\boldsymbol{u}\|_0$ is nothing else but the square root of the kinetic energy. Note that to derive this identity, we needed to invoke the mass conservation equation and the incompressibility of the flow. As a result, the standard form of the momentum equation cannot guarantee that the kinetic energy balance is preserved at the discrete level, because mass conservation and incompressibility cannot be satisfied exactly when discretized. To avoid this difficulty we propose now an alternative form of the momentum equation.

The arguments above show clearly that it is convenient to introduce the auxiliary variable $\sigma = \sqrt{\rho}$. By writing $\rho\boldsymbol{u} = \sigma\sigma\boldsymbol{u}$ in the momentum equation, a direct calculation, using the identity $\sigma\frac{\partial\sigma}{\partial t} = \frac{1}{2}\frac{\partial\rho}{\partial t}$ together with the mass conservation equation in its canonical form (2.1), gives the equivalent equation

$$\sigma\frac{\partial(\sigma\boldsymbol{u})}{\partial t} + (\rho\boldsymbol{u}\cdot\boldsymbol{\nabla})\boldsymbol{u} + \frac{\boldsymbol{u}}{2}\boldsymbol{\nabla}\cdot(\rho\boldsymbol{u}) - \mu\nabla^2\boldsymbol{u} + \boldsymbol{\nabla}P = \boldsymbol{f}. \tag{2.9}$$

By using the vector conterpart of Lemma 1, one verifies that this alternative form of the momentum equation yields (2.8) without invoking mass conservation nor incompressibility.

As a result (2.9) will preserve exactly the kinetic energy balance at the discrete level. Note that in the particular case of uniform density the nonlinear terms in Eq. (2.9) are written exactly in the skew-symmetric form which is well known for yielding unconditional stability in the incompressible Navier–Stokes equations [13].

In conclusion, the complete system of equations for developing unconditionally stable integration schemes for variable density incompressible flows is written in the form

$$\begin{gathered} \frac{\partial \rho}{\partial t} + \boldsymbol{u} \cdot \boldsymbol{\nabla} \rho + \frac{\rho}{2} \boldsymbol{\nabla} \cdot \boldsymbol{u} = 0, \\ \sigma \frac{\partial (\sigma \boldsymbol{u})}{\partial t} + (\rho \boldsymbol{u} \cdot \boldsymbol{\nabla}) \boldsymbol{u} + \frac{\boldsymbol{u}}{2} \boldsymbol{\nabla} \cdot (\rho \boldsymbol{u}) - \mu \nabla^2 \boldsymbol{u} + \boldsymbol{\nabla} P = \boldsymbol{f}, \\ \boldsymbol{\nabla} \cdot \boldsymbol{u} = 0, \end{gathered} \tag{2.10}$$

where $\sigma = \sqrt{\rho}$, by definition.

3. NONINCREMENTAL PROJECTION METHOD FOR VARIABLE DENSITY

To realize the main differences between the classical projection method for a homogeneous fluid and the projection method proposed here for variable-density incompressible flows, we concentrate first on the simplest fractional step method, that is, the original (nonincremental) version of the method. This method is characterized by a time-splitting error of first order, which renders it useless for developing projection schemes of second order accuracy in time. As shown in [5], second order accuracy in time can be achieved only by using the incremental technique, also known as the pressure correction method (to be discussed in Section 4). For the sake of simplicity of the arguments, in the present section we restrict ourselves to the nonincremental method, which allows us to establish features present also in the more accurate incremental method. We now briefly restate some previously established results [9, 11, 12] and introduce the necessary notations. In particular we focus on the difference in terms of functional setting existing between the two substeps of the method, namely the viscous step and the projection step. This distinction leads to consider two different vector spaces for approximating the intermediate velocity and the end-of-step velocity.

3.1. *The Nonincremental Scheme for Variable Density Flows*

The main idea of the fractional step projection method is the splitting of the viscosity from the incompressibility, which are dealt with in two separate subsequent steps. To implement the same idea in the context of variable-density flows, we insist on the idea of decoupling the mass conservation equation also, solving this equation in the first fractional step of the method.

Let us set $\rho^0 = \rho_0$, $\sigma^0 = \sqrt{\rho_0}$ and $\boldsymbol{u}^0 = \boldsymbol{u}_0$. By considering an implicit treatment of the unknown ρ and an explicit account of the advection velocity (semi-implicit scheme), the time discretization of the transport mass equation gives

$$\begin{gathered} \frac{\rho^{n+1} - \rho^n}{\Delta t} + \boldsymbol{u}^n \cdot \boldsymbol{\nabla} \rho^{n+1} + \frac{1}{2} (\boldsymbol{\nabla} \cdot \boldsymbol{u}^n) \rho^{n+1} = 0, \\ \rho^{n+1}|_{\Gamma_{\text{in}}} = a^{n+1}, \end{gathered} \tag{3.1}$$

where $a^{n+1} = a(t_{n+1})$. Once ρ^{n+1} has been determined, define $\sigma^{n+1} = \sqrt{\rho^{n+1}}$. Then, solve the following problem of the viscous (advection–diffusion) step to determine the intermediate[1] velocity $\boldsymbol{u}^{n+1}$,

$$\sigma^{n+1}\frac{\sigma^{n+1}\boldsymbol{u}^{n+1} - \sigma^n\hat{\boldsymbol{u}}^n}{\Delta t} - \mu\nabla^2\boldsymbol{u}^{n+1} + (\rho^{n+1}\boldsymbol{u}^n \cdot \boldsymbol{\nabla})\boldsymbol{u}^{n+1} + \frac{1}{2}[\boldsymbol{\nabla}\cdot(\rho^{n+1}\boldsymbol{u}^n)]\boldsymbol{u}^{n+1} = \boldsymbol{f}^{n+1},$$
$$\boldsymbol{u}^{n+1}|_\Gamma = \boldsymbol{b}^{n+1}, \tag{3.2}$$

where $\boldsymbol{b}^{n+1} = \boldsymbol{b}(t_{n+1})$. Finally, having determined the intermediate velocity $\boldsymbol{u}^{n+1}$, we have to perform the projection step,

$$\rho^{n+1}\frac{\hat{\boldsymbol{u}}^{n+1} - \boldsymbol{u}^{n+1}}{\Delta t} + \hat{\boldsymbol{\nabla}}P^{n+1} = 0,$$
$$\hat{\boldsymbol{\nabla}}\cdot\hat{\boldsymbol{u}}^{n+1} = 0, \tag{3.3}$$
$$\boldsymbol{n}\cdot\hat{\boldsymbol{u}}^{n+1}|_\Gamma = \boldsymbol{n}\cdot\boldsymbol{b}^{n+1},$$

to determine the end-of-step velocity $\hat{\boldsymbol{u}}^{n+1}$ and the pressure P^{n+1}. It is important to note the structural difference existing between the viscous step (3.2) and the projection phase of (3.3) of the calculation. The former constitutes an elliptic boundary value problem for an intermediate velocity $\hat{\boldsymbol{u}}^{n+1}$ accounting for viscosity and convection, whereas the latter represents an essentially inviscid problem which determines the end-of-step velocity $\hat{\boldsymbol{u}}^{n+1}$ together with a suitable approximation of the pressure P^{n+1} so that the incompressibility constraint is satisfied. As a consequence, boundary conditions of a different kind are imposed on the velocity unknowns that are calculated in the two half-steps. Accordingly, the two operators $\boldsymbol{\nabla}\cdot$ and $\hat{\boldsymbol{\nabla}}\cdot$ occurring in the two steps are distinct since they act on vector fields belonging to spaces which are endowed with very different regularities, namely, $\boldsymbol{H}^1$ for the intermediate velocity $\boldsymbol{u}$ and $\boldsymbol{H}^{\mathrm{div}}$ (or possibly $\boldsymbol{L}^2$) for the end-of-step velocity $\hat{\boldsymbol{u}}$.

The time integration scheme chosen in the momentum equation is fully implicit for the viscous term and semi-implicit for the advection term. This scheme is unconditionally stable; i.e., it avoids any restriction on the time step Δt, as stated formally by the following proposition:

PROPOSITION 1. *For any $\Delta t > 0$, the solution $(\rho^n, \boldsymbol{u}^n, P^n)$, $n = 1, 2, \ldots$, of the semi-discrete fractional-step equations* (3.1)–(3.3) *with $\boldsymbol{f} = 0$ satisfies the stability estimate*

$$\|\rho^{n+1}\|_0 \le \|\rho_0\|_0, \quad \|\sigma^{n+1}\boldsymbol{u}^{n+1}\|_0^2 + 2\mu\Delta t\sum_{k=0}^{n}\|\boldsymbol{\nabla}\boldsymbol{u}^{k+1}\|_0^2 \le \|\sigma_0\boldsymbol{u}_0\|_0^2.$$

Proof. We first multiply (3.1) by $2\Delta t\rho^{n+1}$ and integrate over Ω. Using $\boldsymbol{n}\cdot\boldsymbol{u}^n|_\Gamma = 0$, $\forall\boldsymbol{u}^n$, and the identity $2a(a-b) = a^2 + (a-b)^2 - b^2$, we have

$$\|\rho^{n+1}\|_0^2 + \|\rho^{n+1} - \rho^n\|_0^2 - \|\rho^n\|_0^2 = 0,$$

and therefore

$$\|\rho^{n+1}\|_0 \le \|\rho_0\|_0.$$

[1] We use $\boldsymbol{u}$ to indicate the intermediate velocity for notational simplicity, since, as will become clear later, this velocity is the only one necessary in the final computational algorithm.

Multipling the first equation (3.2) of the viscous step (with $\boldsymbol{f} = 0$, for simplicity) by $2\Delta t\boldsymbol{u}^{n+1}$ and integrating over Ω, using $\boldsymbol{u}^n|_\Gamma = 0$, $\forall \boldsymbol{u}^n$, we have

$$\|\sigma^{n+1}\boldsymbol{u}^{n+1}\|_0^2 + \|\sigma^{n+1}\boldsymbol{u}^{n+1} - \sigma^n\hat{\boldsymbol{u}}^n\|_0^2 - \|\sigma^n\hat{\boldsymbol{u}}^n\|_0^2 + 2\Delta t\mu\|\boldsymbol{\nabla}\boldsymbol{u}^{n+1}\|_0^2 = 0.$$

Multiplying the momentum equation (3.3) of the projection step by $2\Delta t\hat{\boldsymbol{u}}^{n+1}$ and using both $\hat{\boldsymbol{\nabla}}\cdot\hat{\boldsymbol{u}}^{n+1} = 0$ and $\boldsymbol{n}\cdot\hat{\boldsymbol{u}}^{n+1}|_\Gamma = 0$, we deduce

$$\|\sigma^{n+1}\hat{\boldsymbol{u}}^{n+1}\|_0^2 + \|\sigma^{n+1}(\hat{\boldsymbol{u}}^{n+1} - \boldsymbol{u}^{n+1})\|_0^2 = \|\sigma^{n+1}\boldsymbol{u}^{n+1}\|_0^2.$$

Then, adding the last two equations, we obtain

$$\begin{aligned}&\|\sigma^{n+1}\boldsymbol{u}^{n+1} - \sigma^n\hat{\boldsymbol{u}}^n\|_0^2 + 2\Delta t\mu\|\boldsymbol{\nabla}\boldsymbol{u}^{n+1}\|_0^2 + \|\sigma^{n+1}\hat{\boldsymbol{u}}^{n+1}\|_0^2\\ &\quad + \|\sigma^{n+1}(\hat{\boldsymbol{u}}^{n+1} - \boldsymbol{u}^{n+1})\|_0^2 = \|\sigma^n\hat{\boldsymbol{u}}^n\|_0^2,\end{aligned}$$

and therefore

$$\|\sigma^{n+1}\hat{\boldsymbol{u}}^{n+1}\|_0^2 + 2\Delta t\mu\|\boldsymbol{\nabla}\boldsymbol{u}^{n+1}\|_0^2 \le \|\sigma^n\hat{\boldsymbol{u}}^n\|_0^2.$$

The desired result follows easily. ■

3.2. *Elliptic Pressure Equation and Elimination of the End-of-Step Velocity*

Dividing the first equation of the projection step (3.3) by ρ^{n+1} and then applying $\hat{\boldsymbol{\nabla}}\cdot$ to the resulting equation, we obtain the following Neumann boundary value problem for the pressure P^{n+1},

$$\begin{aligned}-\hat{\boldsymbol{\nabla}}\cdot\left(\frac{1}{\rho^{n+1}}\hat{\boldsymbol{\nabla}}P^{n+1}\right) &= -(\Delta t)^{-1}\boldsymbol{\nabla}\cdot\boldsymbol{u}^{n+1},\\ \left.\frac{\partial P^{n+1}}{\partial n}\right|_\Gamma &= 0,\end{aligned} \tag{3.4}$$

where we have used $\hat{\boldsymbol{\nabla}}\cdot\boldsymbol{u} = \boldsymbol{\nabla}\cdot\boldsymbol{u}$ (owing to the fact that in mathematical terms $\hat{\boldsymbol{\nabla}}\cdot$ is an extension of $\hat{\boldsymbol{\nabla}}\cdot$). The weak form of the elliptic problem for pressure in the incompressible step reads

$$\forall w \in H^1(\Omega),\quad \left(\hat{\boldsymbol{\nabla}}w, \frac{1}{\rho^{n+1}}\hat{\boldsymbol{\nabla}}P^{n+1}\right) = -\frac{(w, \boldsymbol{\nabla}\cdot\boldsymbol{u}^{n+1})}{\Delta t} = \frac{(\hat{\boldsymbol{\nabla}}w, \boldsymbol{u}^{n+1})}{\Delta t}.$$

Once P^{n+1} is known, the end-of-step velocity is given by the explicit relation

$$\hat{\boldsymbol{u}}^{n+1} = \boldsymbol{u}^{n+1} - \frac{\Delta t}{\rho^{n+1}}\hat{\boldsymbol{\nabla}}P^{n+1}. \tag{3.5}$$

Note that, insofar as the pressure solution of the Poisson-like equation above is in H^1, $\hat{\boldsymbol{\nabla}}P^{n+1}$ belongs to $\boldsymbol{L}^2$; as a result, $\hat{\boldsymbol{u}}^{n+1}$ should *not* be expected *a priori* to have more regularity than that of $\boldsymbol{H}^{\mathrm{div}}$ (which is lower than that of $\boldsymbol{H}^1$).

The important point is now that the discontinuous (distributional) end-of-step velocity $\hat{\boldsymbol{u}}^{n+1}$ can be made to disappear completely from the computational algorithm to be implemented. In fact, using

$$\hat{\boldsymbol{u}}^n = \boldsymbol{u}^n - \frac{\Delta t}{\rho^n}\hat{\boldsymbol{\nabla}} P^n$$

in the evolutionary term of the momentum equation of the viscous step (3.2), we obtain

$$\begin{aligned}
&\sigma^{n+1}\frac{\sigma^{n+1}\boldsymbol{u}^{n+1} - \sigma^n \hat{\boldsymbol{u}}^n}{\Delta t} \\
&\quad = \sigma^{n+1}\frac{\sigma^{n+1}\boldsymbol{u}^{n+1} - \sigma^n\left[\boldsymbol{u}^n - \frac{\Delta t}{\rho^n}\hat{\boldsymbol{\nabla}} P^n\right]}{\Delta t} \\
&\quad = \sigma^{n+1}\frac{\sigma^{n+1}\boldsymbol{u}^{n+1} - \sigma^n \boldsymbol{u}^n}{\Delta t} + \frac{\sigma^{n+1}}{\sigma^n}\hat{\boldsymbol{\nabla}} P^n \\
&\quad = \frac{\rho^{n+1}\boldsymbol{u}^{n+1} - \sigma^{n+1}\sigma^n \boldsymbol{u}^n}{\Delta t} + \frac{\sigma^{n+1}}{\sigma^n}\hat{\boldsymbol{\nabla}} P^n.
\end{aligned}$$

This result can be substituted into the momentum equation of the viscous step. As a consequence, the three uncoupled problems to be solved in the nonincremental fractional step projection method for variable density flows are rewritten here in their final form:

$$\begin{gathered}
\frac{\rho^{n+1} - \rho^n}{\Delta t} + \boldsymbol{u}^n \cdot \boldsymbol{\nabla}\rho^{n+1} + \frac{1}{2}(\boldsymbol{\nabla}\cdot\boldsymbol{u}^n)\rho^{n+1} = 0, \\
\rho^{n+1}|_{\Gamma_{\text{in}}} = a^{n+1};
\end{gathered} \tag{3.6}$$

$$\begin{aligned}
&\frac{\rho^{n+1}\boldsymbol{u}^{n+1} - \sigma^{n+1}\sigma^n \boldsymbol{u}^n}{\Delta t} - \mu\nabla^2\boldsymbol{u}^{n+1} + (\rho^{n+1}\boldsymbol{u}^n \cdot \boldsymbol{\nabla})\boldsymbol{u}^{n+1} \\
&\quad + \frac{1}{2}[\boldsymbol{\nabla}\cdot(\rho^{n+1}\boldsymbol{u}^n)]\boldsymbol{u}^{n+1} = -\frac{\sigma^{n+1}}{\sigma^n}\boldsymbol{\nabla} P^n + \boldsymbol{f}^{n+1},
\end{aligned} \tag{3.7}$$

$$\boldsymbol{u}^{n+1}|_\Gamma = \boldsymbol{b}^{n+1};$$

$$\begin{gathered}
-\hat{\boldsymbol{\nabla}}\cdot\left(\frac{1}{\rho^{n+1}}\hat{\boldsymbol{\nabla}} P^{n+1}\right) = -(\Delta t)^{-1}\boldsymbol{\nabla}\cdot\boldsymbol{u}^{n+1}, \\
\left.\frac{\partial P^{n+1}}{\partial n}\right|_\Gamma = 0.
\end{gathered} \tag{3.8}$$

3.3. *Weak Form of the Equations*

Let us introduce a finite element approximation $Y_h \subset H^1$ for the density ρ_h, $\boldsymbol{X}_{0,h} \subset \boldsymbol{H}_0^1$ for the intermediate velocity $\boldsymbol{u}_h$, and $N_h \subset H^1$ for the pressure P_h, each pressure field being defined up to a constant.

The weak formulation of the mass conservation step (3.6) reads: For $n \geq 0$, find $\rho_h^{n+1} \in Y_h$ such that $\rho_h^{n+1}|_{\Gamma_{\text{in}}} = a^{n+1}$ and such that, for all $v_h \in Y_h$ with $v_h|_{\Gamma_{\text{in}}} = 0$,

$$\left(v_h, \frac{\rho_h^{n+1} - \rho_h^n}{\Delta t}\right) + \left(v_h, \boldsymbol{u}_h^n \cdot \boldsymbol{\nabla}\rho_h^{n+1} + \frac{1}{2}(\boldsymbol{\nabla}\cdot\boldsymbol{u}_h^n)\rho_h^{n+1}\right) = 0. \tag{3.9}$$

Of course, the solution of the discrete equation (3.9) presents the well-known difficulties pertaining to any Galerkin finite element approximation to hyperbolic problems. To avoid

the spurious spatial oscillations induced by the Galerkin technique, we have used a new stabilization procedure proposed in [6]. This technique basically amounts to a two-level decomposition of the finite element space Y_h to add a nonlinear diffusion term to the equation (3.9) as follows

$$\left(v_h, \frac{\rho_h^{n+1}-\rho_h^n}{\Delta t}\right) + \left(v_h, \boldsymbol{u}_h^n \cdot \boldsymbol{\nabla}\rho_h^{n+1} + \frac{1}{2}\left(\boldsymbol{\nabla}\cdot\boldsymbol{u}_h^n\right)\rho_h^{n+1}\right) = b_h\left(v_h, \rho_h^n, \rho_h^n\right),$$

where $b_h(v_h, \rho_h, \rho_h)$ is a trilinear form of order h^{k+1} when ρ_h is smooth, k being the order of interpolation of the density. For a detailed description of this subgrid stabilization technique the reader is referred to [6].

From the solution ρ_h^{n+1} we compute $\sigma_h^{n+1} = \sqrt{\rho_h^{n+1}}$. Then, the weak formulation of the advection–diffusion step (3.7) reads: For $n \geq 0$, find $\boldsymbol{u}_h^{n+1} \in \boldsymbol{X}_{\boldsymbol{b}^{n+1},h}$ such that, for all $\boldsymbol{v}_h \in \boldsymbol{X}_{0,h}$,

$$\left(\boldsymbol{v}_h, \frac{\rho_h^{n+1}\boldsymbol{u}_h^{n+1} - \sigma_h^{n+1}\sigma_h^n\boldsymbol{u}_h^n}{\Delta t}\right) + \mu\left(\boldsymbol{\nabla}\boldsymbol{v}_h, \boldsymbol{\nabla}\boldsymbol{u}_h^{n+1}\right) + \left(\boldsymbol{v}_h, \left(\rho_h^{n+1}\boldsymbol{u}_h^n\cdot\boldsymbol{\nabla}\right)\boldsymbol{u}_h^{n+1}\right)$$
$$+ \frac{1}{2}\left(\boldsymbol{v}_h, \left[\boldsymbol{\nabla}\cdot\left(\rho_h^{n+1}\boldsymbol{u}_h^n\right)\right]\boldsymbol{u}_h^{n+1}\right) = -\left(\boldsymbol{v}_h, \frac{\sigma_h^{n+1}}{\sigma_h^n}\boldsymbol{\nabla}P_h^n\right) + \left(\boldsymbol{v}_h, \boldsymbol{f}^{n+1}\right). \tag{3.10}$$

The projection step has a unique expression only once the functional space for the end-of-step velocity is chosen. As shown in [4], many options are possible; one of the simplest consists in selecting $\hat{\boldsymbol{u}}_h^{n+1}$ in $\boldsymbol{X}_h + \boldsymbol{\nabla}N_h$. Given this particular choice, it can be proven that the operator $\hat{\boldsymbol{\nabla}}_h$, the discrete counterpart of $\hat{\boldsymbol{\nabla}}$, coincides exactly with the restriction to N_h of the gradient operator (in terms of distributions); as a result, the spatially discrete version of the projection step takes the following form: For $n \geq 0$, find $P_h^{n+1} \in N_h$ such that, for all $w_h \in N_h$,

$$\left(\boldsymbol{\nabla}w_h, \frac{1}{I_h\left[\rho_h^{n+1}\right]}\boldsymbol{\nabla}P_h^{n+1}\right) = -(\Delta t)^{-1}\left(w_h, \boldsymbol{\nabla}\cdot\boldsymbol{u}_h^{n+1}\right), \tag{3.11}$$

where the variable coefficient ρ_h^{n+1} in the elliptic operator has been replaced by its injection $I_h[\rho_h^{n+1}]$ into the discrete space N_h of the pressure variable.

Note that, by virtue of the σ- and skew symmetric form of the momentum equation, the spatially discrete equations of the proposed projection method inherit directly the same stability properties as those of the spatially continuous problem.

4. INCREMENTAL PROJECTION METHOD FOR VARIABLE DENSITY

We turn now to the incremental version of the projection method, which has been demonstrated to be a possible way for developing second order accurate truly projection schemes for simulating incompressible viscous flows. Our goal is to obtain a scheme that preserves the unconditional stability of the nonincremental scheme, considered in the previous section. The extension of the incremental projection method established for homogeneous incompressible flows to the variable density case is however not immediate because of the presence of the weight $1/\rho^{n+1}(\boldsymbol{x})$ in the equation of the projection step.

4.1. *Pressure Adaptation Step for Variable Density*

To deal with such a difficulty it is necessary to introduce an intermediate step between the mass conservation step and the viscous step. In this step, starting from an approximate version of the pressure denoted by Q^n obtained in the projection step of the previous time level, one computes a corrected pressure P^{n+1} solution of the elliptic equation

$$-\hat{\boldsymbol{\nabla}} \cdot \left(\frac{1}{\rho^{n+1}} \hat{\boldsymbol{\nabla}} P^{n+1} \right) = -\hat{\boldsymbol{\nabla}} \cdot \left(\frac{1}{\sigma^{n+1}\sigma^n} \hat{\boldsymbol{\nabla}} Q^n \right), \tag{4.1}$$

supplemented by the Neumann boundary condition

$$\frac{1}{\sigma^{n+1}} \frac{\partial P^{n+1}}{\partial n}\bigg|_\Gamma = \frac{1}{\sigma^n} \frac{\partial Q^n}{\partial n}\bigg|_\Gamma. \tag{4.2}$$

The precise role of this unconventional step will be clarified by the subsequent L^2 stability analysis. Note that this pressure adaptation can be interpreted as a preliminary projection step defined by the problem

$$\begin{aligned} \hat{\boldsymbol{u}}_{\text{aux}} + \frac{\hat{\boldsymbol{\nabla}} P^{n+1}}{\rho^{n+1}} &= \frac{\hat{\boldsymbol{\nabla}} Q^n}{\sigma^{n+1}\sigma^n}, \\ \hat{\boldsymbol{\nabla}} \cdot \hat{\boldsymbol{u}}_{\text{aux}} &= 0, \\ \boldsymbol{n} \cdot \hat{\boldsymbol{u}}_{\text{aux}}|_\Gamma &= 0. \end{aligned} \tag{4.3}$$

The equation for the viscous step of the incremental projection method is

$$\begin{aligned} \sigma^{n+1} \frac{\sigma^{n+1}\boldsymbol{u}^{n+1} - \sigma^n \hat{\boldsymbol{u}}^n}{\Delta t} - \mu \nabla^2 \boldsymbol{u}^{n+1} + (\rho^{n+1}\boldsymbol{u}^n \cdot \boldsymbol{\nabla})\boldsymbol{u}^{n+1} \\ + \frac{1}{2}[\boldsymbol{\nabla} \cdot (\rho^{n+1}\boldsymbol{u}^n)]\boldsymbol{u}^{n+1} = -\boldsymbol{\nabla} P^{n+1} + \boldsymbol{f}^{n+1}, \\ \boldsymbol{u}^{n+1}|_\Gamma = \boldsymbol{b}^{n+1}. \end{aligned} \tag{4.4}$$

Finally, the projection step of the incremental scheme is written as

$$\begin{aligned} \rho^{n+1} \frac{\hat{\boldsymbol{u}}^{n+1} - \boldsymbol{u}^{n+1}}{\Delta t} + \hat{\boldsymbol{\nabla}}(Q^{n+1} - P^{n+1}) = 0, \\ \hat{\boldsymbol{\nabla}} \cdot \hat{\boldsymbol{u}}^{n+1} = 0, \\ \boldsymbol{n} \cdot \hat{\boldsymbol{u}}^{n+1}|_\Gamma = \boldsymbol{n} \cdot \boldsymbol{b}^{n+1}, \end{aligned} \tag{4.5}$$

where P^{n+1} has been calculated in the pressure adaptation step of the current time level.

4.2. *The Incremental Scheme for Variable Density Flows*

The set of equations performing one entire time step of the incremental projection method can be obtained as in the nonincremental method by writing the projection step in the form of a Neumann problem for a Poisson-like equation and eliminating the end-of-step velocity. A possible scheme, based on a semi-implicit stabilized treatment of the nonlinear term of the mass conservation equation and a unconditionally stable treatment for the momentum

equation of the viscous step, would lead to the following set of four uncoupled problems:

$$\frac{\rho^{n+1}-\rho^n}{\Delta t}+\boldsymbol{u}^n\cdot\boldsymbol{\nabla}\rho^{n+1}+\frac{1}{2}(\boldsymbol{\nabla}\cdot\boldsymbol{u}^n)\rho^{n+1}=0,\qquad \rho^{n+1}|_{\Gamma_{\text{in}}}=a^{n+1};\tag{4.6}$$

$$-\hat{\boldsymbol{\nabla}}\cdot\left(\frac{1}{\rho^{n+1}}\hat{\boldsymbol{\nabla}}P^{n+1}\right)=-\hat{\boldsymbol{\nabla}}\cdot\left(\frac{1}{\sigma^{n+1}\sigma^n}\hat{\boldsymbol{\nabla}}Q^n\right),\qquad \frac{1}{\sigma^{n+1}}\frac{\partial P^{n+1}}{\partial n}\bigg|_\Gamma=\frac{1}{\sigma^n}\frac{\partial Q^n}{\partial n}\bigg|_\Gamma;\tag{4.7}$$

$$\frac{\rho^{n+1}\boldsymbol{u}^{n+1}-\sigma^{n+1}\sigma^n\boldsymbol{u}^n}{\Delta t}-\mu\nabla^2\boldsymbol{u}^{n+1}+(\rho^{n+1}\boldsymbol{u}^n\cdot\boldsymbol{\nabla})\boldsymbol{u}^{n+1}+\frac{1}{2}[\boldsymbol{\nabla}\cdot(\rho^{n+1}\boldsymbol{u}^n)]\boldsymbol{u}^{n+1}$$
$$=-\boldsymbol{\nabla}P^{n+1}-\frac{\sigma^{n+1}}{\sigma^n}\boldsymbol{\nabla}(Q^n-P^n)+\boldsymbol{f}^{n+1},\qquad \boldsymbol{u}^{n+1}|_\Gamma=\boldsymbol{b}^{n+1};\tag{4.8}$$

$$-\hat{\boldsymbol{\nabla}}\cdot\left(\frac{1}{\rho^{n+1}}\hat{\boldsymbol{\nabla}}(Q^{n+1}-P^{n+1})\right)=-(\Delta t)^{-1}\boldsymbol{\nabla}\cdot\boldsymbol{u}^{n+1},\qquad \frac{\partial(Q^{n+1}-P^{n+1})}{\partial n}\bigg|_\Gamma=0.\tag{4.9}$$

4.3. *Stability of the Incremental Projection Method*

The proof of stability of the incremental projection method proceeds as does that of the nonincremental method but takes into account in an essential way the pressure adaptation equation (4.1). First, multiply this equation by P^{n+1} and integrate over Ω. Using the integration by parts and the Neumann boundary condition (4.2) we obtain, by the Schwartz inequality,

$$\left\|\frac{\hat{\boldsymbol{\nabla}}P^{n+1}}{\sigma^{n+1}}\right\|_0^2=\left(\frac{\hat{\boldsymbol{\nabla}}P^{n+1}}{\sigma^{n+1}},\frac{\hat{\boldsymbol{\nabla}}Q^n}{\sigma^n}\right)\le\left\|\frac{\hat{\boldsymbol{\nabla}}P^{n+1}}{\sigma^{n+1}}\right\|_0\left\|\frac{\hat{\boldsymbol{\nabla}}Q^n}{\sigma^n}\right\|_0,$$

from which it follows immediately that

$$\left\|\frac{\hat{\boldsymbol{\nabla}}P^{n+1}}{\sigma^{n+1}}\right\|_0\le\left\|\frac{\hat{\boldsymbol{\nabla}}Q^n}{\sigma^n}\right\|_0.$$

Then, multiplying the momentum equation (4.4) by $2\Delta t\boldsymbol{u}^{n+1}$ and integrating over Ω, using $\boldsymbol{u}^n|_\Gamma=0,\ \forall\boldsymbol{u}^n$, we have

$$\|\sigma^{n+1}\boldsymbol{u}^{n+1}\|_0^2+\|\sigma^{n+1}\boldsymbol{u}^{n+1}-\sigma^n\hat{\boldsymbol{u}}^n\|_0^2-\|\sigma^n\hat{\boldsymbol{u}}^n\|_0^2$$
$$+2\Delta t\mu\|\boldsymbol{\nabla}\boldsymbol{u}^{n+1}\|_0^2=-2\Delta t\int_\Omega\boldsymbol{u}^{n+1}\cdot\boldsymbol{\nabla}P^{n+1}.$$

Multiplying the momentum equation (4.5) of the projection step by $(2\hat{\boldsymbol{\nabla}}P^{n+1})/\rho^{n+1}$ and using $\hat{\boldsymbol{\nabla}}\cdot\hat{\boldsymbol{u}}^{n+1}=0$, we deduce that

$$-\frac{2}{\Delta t}\int_\Omega\hat{\boldsymbol{\nabla}}P^{n+1}\cdot\boldsymbol{u}^{n+1}+2\int_\Omega\frac{\hat{\boldsymbol{\nabla}}P^{n+1}}{\rho^{n+1}}\cdot\hat{\boldsymbol{\nabla}}(Q^{n+1}-P^{n+1})=0,$$

from which, using again the identity $2a(a-b) = a^2 + (a-b)^2 - b^2$, we obtain

$$-\frac{2}{\Delta t}\int_\Omega \hat{\boldsymbol{\nabla}} P^{n+1}\cdot \boldsymbol{u}^{n+1} - \left\|\frac{\hat{\boldsymbol{\nabla}} P^{n+1}}{\sigma^{n+1}}\right\|_0^2 - \left\|\frac{\hat{\boldsymbol{\nabla}}(Q^{n+1}-P^{n+1})}{\sigma^{n+1}}\right\|_0^2 + \left\|\frac{\hat{\boldsymbol{\nabla}} Q^{n+1}}{\sigma^{n+1}}\right\|_0^2 = 0.$$

Using the inequality established between $(\hat{\boldsymbol{\nabla}} P^{n+1})/\sigma^{n+1}$ and $(\hat{\boldsymbol{\nabla}} Q^n)/\sigma^n$ we obtain

$$\begin{aligned}&-\frac{2}{\Delta t}\int_\Omega \hat{\boldsymbol{\nabla}} P^{n+1}\cdot \boldsymbol{u}^{n+1} + \left\|\frac{\hat{\boldsymbol{\nabla}} Q^{n+1}}{\sigma^{n+1}}\right\|_0^2 - \frac{\|\sigma^{n+1}(\hat{\boldsymbol{u}}^{n+1}-\boldsymbol{u}^{n+1})\|_0^2}{(\Delta t)^2}\\ &= \left\|\frac{\hat{\boldsymbol{\nabla}} P^{n+1}}{\sigma^{n+1}}\right\|_0^2 \le \left\|\frac{\hat{\boldsymbol{\nabla}} Q^{n}}{\sigma^{n}}\right\|_0^2.\end{aligned}$$

Finally, multiplying the first equation of the projection step (4.5), this time by $2\Delta t\hat{\boldsymbol{u}}^{n+1}$, and using $\hat{\boldsymbol{\nabla}}\cdot\hat{\boldsymbol{u}}^{n+1} = 0$ and $\boldsymbol{n}\cdot\hat{\boldsymbol{u}}^{n+1}|_\Gamma = 0$, we obtain

$$\|\sigma^{n+1}\hat{\boldsymbol{u}}^{n+1}\|_0^2 + \|\sigma^{n+1}(\hat{\boldsymbol{u}}^{n+1}-\boldsymbol{u}^{n+1})\|_0^2 = \|\sigma^{n+1}\boldsymbol{u}^{n+1}\|_0^2.$$

Adding now the three relations so obtained, the second one being multiplied by $(\Delta t)^2$, one finally infers that

$$\|\sigma^{n+1}\hat{\boldsymbol{u}}^{n+1}\|_0^2 + (\Delta t)^2\left\|\frac{\hat{\boldsymbol{\nabla}} Q^{n+1}}{\sigma^{n+1}}\right\|_0^2 + 2\Delta t\mu\|\boldsymbol{\nabla}\boldsymbol{u}^{n+1}\|_0^2 \le \|\sigma^n\hat{\boldsymbol{u}}^n\|_0^2 + (\Delta t)^2\left\|\frac{\hat{\boldsymbol{\nabla}} Q^{n}}{\sigma^{n}}\right\|_0^2.$$

As a result we have proved:

PROPOSITION 2. *For any $\Delta t > 0$, the solution $(\rho^n, \boldsymbol{u}^n, P^n)$, $n = 1, 2, \ldots$, of the incremental projection method* (4.6)–(4.9) *with $\boldsymbol{f} = 0$ satisfies the stability estimate*

$$\|\sigma^{n+1}\boldsymbol{u}^{n+1}\|_0^2 + (\Delta t)^2\left\|\frac{\hat{\boldsymbol{\nabla}} Q^{n+1}}{\sigma^{n+1}}\right\|_0^2 + 2\mu\Delta t\sum_{k=0}^{n}\|\boldsymbol{\nabla}\boldsymbol{u}^{k+1}\|_0^2 \le \|\sigma_0\boldsymbol{u}_0\|_0^2 + (\Delta t)^2\left\|\frac{\hat{\boldsymbol{\nabla}} Q_0}{\sigma_0}\right\|_0^2.$$

5. BDF SECOND-ORDER INCREMENTAL PROJECTION METHOD

The incremental projection method introduced in Sections 4.1 and 4.2 has a second-order time-splitting error but to obtain a scheme of second-order accuracy in time it is necessary to replace the two-level semi-implicit time integration algorithm used in the mass conservation and viscous steps by a second-order accurate time stepping method. Following our experience with the projection method for homogeneous incompressible flows [5, 8], we adopt the three-level BDF method. To this aim, we introduce the linearly extrapolated velocity field at the new time level by means of the definition

$$\boldsymbol{u}_\star^{n+1} = 2\boldsymbol{u}^n - \boldsymbol{u}^{n-1}. \tag{5.1}$$

Then, we consider the second-order accurate BDF time integration of the mass conservation

equation

$$\frac{3\rho^{n+1}-4\rho^{n}+\rho^{n-1}}{2\Delta t}+\boldsymbol{u}_{\star}^{n+1}\cdot\boldsymbol{\nabla}\rho^{n+1}+\frac{1}{2}(\boldsymbol{\nabla}\cdot\boldsymbol{u}_{\star}^{n+1})\rho^{n+1}=0. \tag{5.2}$$

Similarly, the momentum equation of the viscous step is integrated in time by the same three-level BDF method, which solves the equation

$$\begin{aligned}\sigma^{n+1}\frac{3\sigma^{n+1}\boldsymbol{u}^{n+1}-4\sigma^{n}\hat{\boldsymbol{u}}^{n}+\sigma^{n-1}\hat{\boldsymbol{u}}^{n-1}}{2\Delta t}-\mu\nabla^{2}\boldsymbol{u}^{n+1}+(\rho^{n+1}\boldsymbol{u}_{\star}^{n+1}\cdot\boldsymbol{\nabla})\boldsymbol{u}^{n+1}\\ +\frac{1}{2}[\boldsymbol{\nabla}\cdot(\rho^{n+1}\boldsymbol{u}_{\star}^{n+1})]\boldsymbol{u}^{n+1}=-\boldsymbol{\nabla}P^{n+1}+\boldsymbol{f}^{n+1}.\end{aligned} \tag{5.3}$$

Finally, the time advancement in the projection step is achieved by means of the equation

$$\rho^{n+1}\frac{3\hat{\boldsymbol{u}}^{n-1}-3\boldsymbol{u}^{n+1}}{2\Delta t}+\hat{\boldsymbol{\nabla}}(Q^{n+1}-P^{n+1})=0. \tag{5.4}$$

Once the projection step is recast into the form of an elliptic equation for the pressure increment and the end-of-step velocity $\hat{\boldsymbol{u}}^{n+1}$ is eliminated, the complete set of uncoupled problems to be solved in the BDF incremental projection method assumes the form

$$\begin{gathered}\frac{3}{2\Delta t}\rho^{n+1}+\boldsymbol{u}_{\star}^{n+1}\cdot\boldsymbol{\nabla}\rho^{n+1}+\frac{1}{2}(\boldsymbol{\nabla}\cdot\boldsymbol{u}_{\star}^{n+1})\rho^{n+1}=\frac{4\rho^{n}-\rho^{n-1}}{2\Delta t},\\ \rho^{n+1}|_{\Gamma_{\mathrm{in}}}=a^{n+1};\end{gathered} \tag{5.5}$$

$$\begin{gathered}-\hat{\boldsymbol{\nabla}}\cdot\left(\frac{1}{\rho^{n+1}}\hat{\boldsymbol{\nabla}}P^{n+1}\right)=-\hat{\boldsymbol{\nabla}}\cdot\left(\frac{1}{\sigma^{n+1}\sigma^{n}}\hat{\boldsymbol{\nabla}}Q^{n}\right),\\ \frac{1}{\sigma^{n+1}}\frac{\partial P^{n+1}}{\partial n}\bigg|_{\Gamma}=\frac{1}{\sigma^{n}}\frac{\partial Q^{n}}{\partial n}\bigg|_{\Gamma};\end{gathered} \tag{5.6}$$

$$\begin{aligned}\frac{3\rho^{n+1}}{2\Delta t}\boldsymbol{u}^{n+1}-\mu\nabla^{2}\boldsymbol{u}^{n+1}+(\rho^{n+1}\boldsymbol{u}_{\star}^{n+1}\cdot\boldsymbol{\nabla})\boldsymbol{u}^{n+1}+\frac{1}{2}[\boldsymbol{\nabla}\cdot(\rho^{n+1}\boldsymbol{u}_{\star}^{n+1})]\boldsymbol{u}^{n+1}\\ =\frac{2}{\Delta t}\sigma^{n+1}\sigma^{n}\boldsymbol{u}^{n}-\frac{1}{2\Delta t}\sigma^{n+1}\sigma^{n-1}\boldsymbol{u}^{n-1}+\boldsymbol{f}^{n+1}-\boldsymbol{\nabla}P^{n+1}\\ -\frac{4\sigma^{n+1}}{3\sigma^{n}}\boldsymbol{\nabla}(Q^{n}-P^{n})+\frac{\sigma^{n+1}}{3\sigma^{n-1}}\boldsymbol{\nabla}(Q^{n-1}-P^{n-1}),\end{aligned} \tag{5.7}$$

$$\begin{gathered}\boldsymbol{u}^{n+1}|_{\Gamma}=\boldsymbol{b}^{n+1};\\ -\hat{\boldsymbol{\nabla}}\cdot\left(\frac{1}{\rho^{n+1}}\hat{\boldsymbol{\nabla}}(Q^{n+1}-P^{n+1})\right)=-\frac{3}{2\Delta t}\boldsymbol{\nabla}\cdot\boldsymbol{u}^{n+1},\\ \frac{\partial(Q^{n+1}-P^{n+1})}{\partial n}\bigg|_{\Gamma}=0;\end{gathered} \tag{5.8}$$

6. NUMERICAL RESULTS

All the numerical results reported hereafter have been obtained using $\mathbb{P}_2$–$\mathbb{P}_1$ finite elements.

6.1. *Error Estimates*

To verify the theoretical $\mathcal{O}((\Delta t)^2)$ accuracy of the three-level BDF projection method, we have tested it against the analytical solution in the unit circle $|\boldsymbol{r}| \leq 1$

$$\begin{aligned} \rho(\boldsymbol{r}, t) &= \rho_1(r, \theta - \sin t), \\ \boldsymbol{u}(\boldsymbol{r}, t) &= (-y\hat{\boldsymbol{x}} + x\hat{\boldsymbol{y}}) \cos t, \\ P(\boldsymbol{r}, t) &= \sin x \sin y \sin t, \end{aligned} \tag{6.1}$$

where $\rho_1(r, \theta)$ is an arbitrary function. In the tests, we used $\rho_1(r, \alpha) = 2 + r \cos \alpha$. The fields $\rho(\boldsymbol{r}, t)$ and $\boldsymbol{u}(\boldsymbol{r}, t)$ satisfy the mass conservation equation identically and $\boldsymbol{u}(\boldsymbol{r}, t)$ is solenoidal. The momentum equation is satisfied by the body force defined by

$$\boldsymbol{f}(\boldsymbol{r}, t) = \begin{pmatrix} (y \sin t - x \cos^2 t)\rho(\boldsymbol{r}, t) + \cos x \sin y \sin t \\ -(x \sin t + y \cos^2 t)\rho(\boldsymbol{r}, t) + \sin x \cos y \sin t \end{pmatrix}. \tag{6.2}$$

The computation have been performed for $0 \leq t \leq 1$. The convergence results are plotted in Fig. 1. We have measured the maximum in time of the L^2 norm of the errors of all variables. The mesh has been chosen fine enough so that the consistency error in space is significantly smaller than that in time. The second-order convergence with respect to Δt is verified in the range $0.01 \leq \Delta t \leq 0.2$.

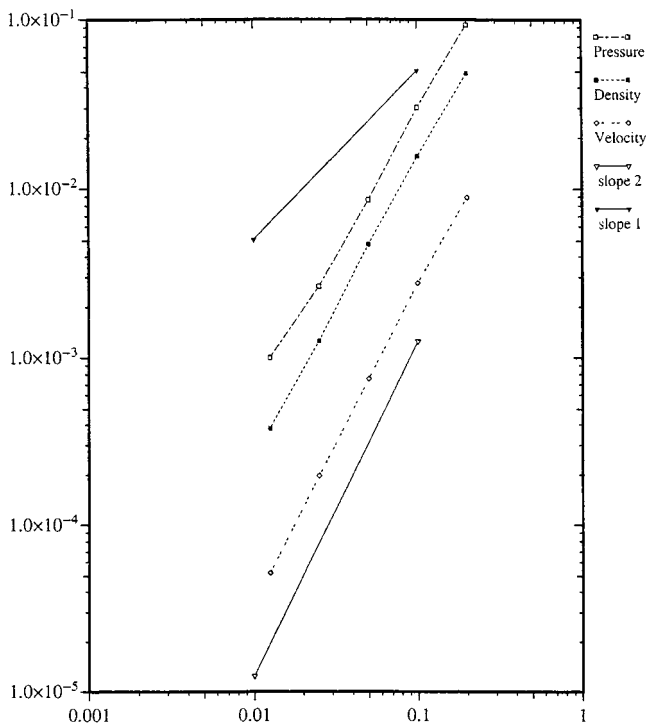

FIG. 1. Maximum in time of the error in the L^2 norm for different time steps.

6.2. *A Low Atwood Number Problem*

As a first test case we have computed the development of a Rayleigh–Taylor instability in the viscous regime. Our starting point is the problem documented by Tryggvason [15]. This problem consists of two layers of fluid initially at rest in the gravity field in $\Omega =]-d/2, d/2[\times]-2d, 2d[$. The initial position of the perturbed interface is $\eta(x) = -0.1d\cos(2\pi x/d)$. The heavy fluid is above and the density ratio is 3. so that the Atwood number is 0.5 according to Tryggvason's definition $\mathrm{At} = (\rho_{\max} - \rho_{\min})/(\rho_{\max} + \rho_{\min})$. The transition between the two fluids is regularized by means of the law

$$\frac{\rho(x, y, t = 0)}{\rho_{\min}} = 2 + \tanh\left(\frac{y - \eta(x)}{0.01d}\right).$$

The governing equations are made dimensionless by using the following references: $\rho_{\min}$ for density, d for length, and $d^{1/2}/g^{1/2}$ for time, where g is the gravity field, so that the reference velocity is $d^{1/2}g^{1/2}$, and the Reynolds number is defined by $\mathrm{Re} = \rho_{\min} d^{3/2} g^{1/2}/\mu$. Assuming the symmetry of the initial condition is maintained during the time evolution, the computational domain has been restricted to $]0, d/2[\times]-2d, 2d[$. A no-slip condition is enforced at the bottom and top walls while symmetry is imposed on the two vertical sides.

The time evolution of the interface of the density field for $\mathrm{Re} = 1000$ is plotted in Fig. 2 at times 1, 1.5, 1.75, 2, 2.25, 2.5 in the time scale of Tryggvason which is related to ours by $t_{\mathrm{Tryg}} = t\sqrt{\mathrm{At}}$. We show the computation on two grids with 21,051 and 30,189 $\mathbb{P}_2$ nodes to give an idea of the convergence with respect to the spatial discretization. We have chosen $\Delta t_{\mathrm{Tryg}} = 5 \times 10^{-4}$. The solutions on the two meshes are consistent in that they show similar structures and differ only in fine details at large time.

To further assess the sensitivity of the method to spatial resolution and to verify that the artificial viscosity is much smaller than the physical viscosity we have solved the same problem for $\mathrm{Re} = 5000$. In Fig. 3, we show the evolution of the interface computed using two meshes composed of 30,189 and 49,577 $\mathbb{P}_2$ nodes, respectively. First, by comparing the solutions obtained for $\mathrm{Re} = 1000$ and $\mathrm{Re} = 5000$ on the grid composed of 30,189 $\mathbb{P}_2$ nodes, we clearly see that the artificial viscosity is much smaller than the physical one, since the two sets of figures are significantly different. Second, by comparing the solutions at $\mathrm{Re} = 5000$ on the two grids, we see that they are in very good agreement in the early stage of the time evolution ($t \leq 1.75$). Some noticeable differences occur at later times and consist in the development of structures within the main vortex that are more complex on the fine mesh than on the coarse one. When comparing the solutions at $t = 2.5$, we observe some disagreement in the shape of the roll-up of the rising bubble, but fair agreement in the overall shape (external and internal) of the falling bubble. A tentative explanation of the delay in the formation of the roll-up of the rising bubble is given at the end of the next section.

We compare now the viscous solutions, $\mathrm{Re} = 1000$ and $\mathrm{Re} = 5000$, with the inviscid one computed in [15]. In Fig. 4, we show the position of the interface of the rising and falling bubble as a function of time. The solid line is the inviscid results from the finest mesh in [15, Fig. 6(a)]. The positions predicted by the projection method for $\mathrm{Re} = 1000$ and $\mathrm{Re} = 5000$ are almost coincident and are in fair agreement with the reference values. We notice though that the velocity of the falling bubble is somewhat higher in our calculations than in [15]. The computational domain used in [15] is $\Omega =]-d/2, d/2[\times]-d, d[$; as a

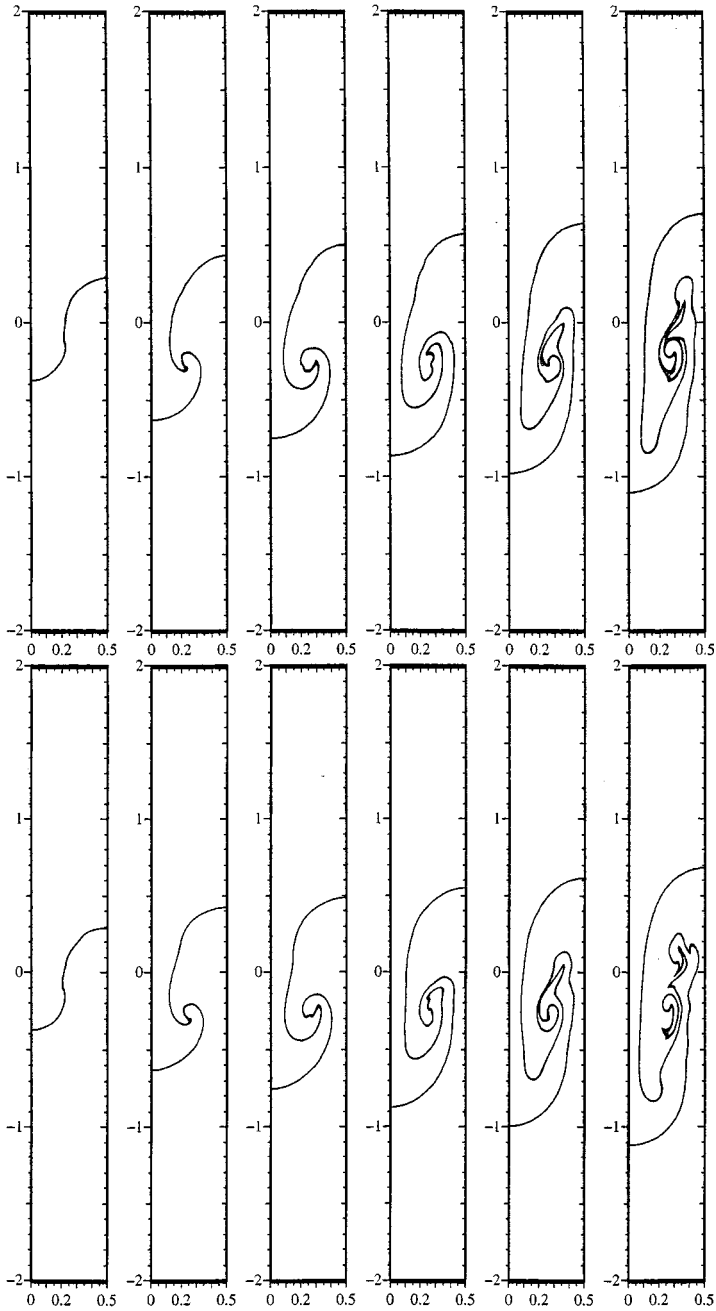

FIG. 2. Re = 1000; density ratio 3. The grid is composed of 21,051 $\mathbb{P}_2$ nodes (top) and 30,189 $\mathbb{P}_2$ nodes (bottom). The initial amplitude is 10% of the wavelength. The interface is shown at times 1, 1.5, 1.75, 2, 2.25, and 2.5 (density contours $1.4 \leq \rho \leq 1.6$).

result, the asymptotic velocity of the falling bubble in the inviscid simulation is reduced because of the presence of the lower no-through flow boundary.

Coming to the comparison of the vortex structure, there is satisfactory agreement of the global characteristics of the flow between the viscous solutions and the inviscid one

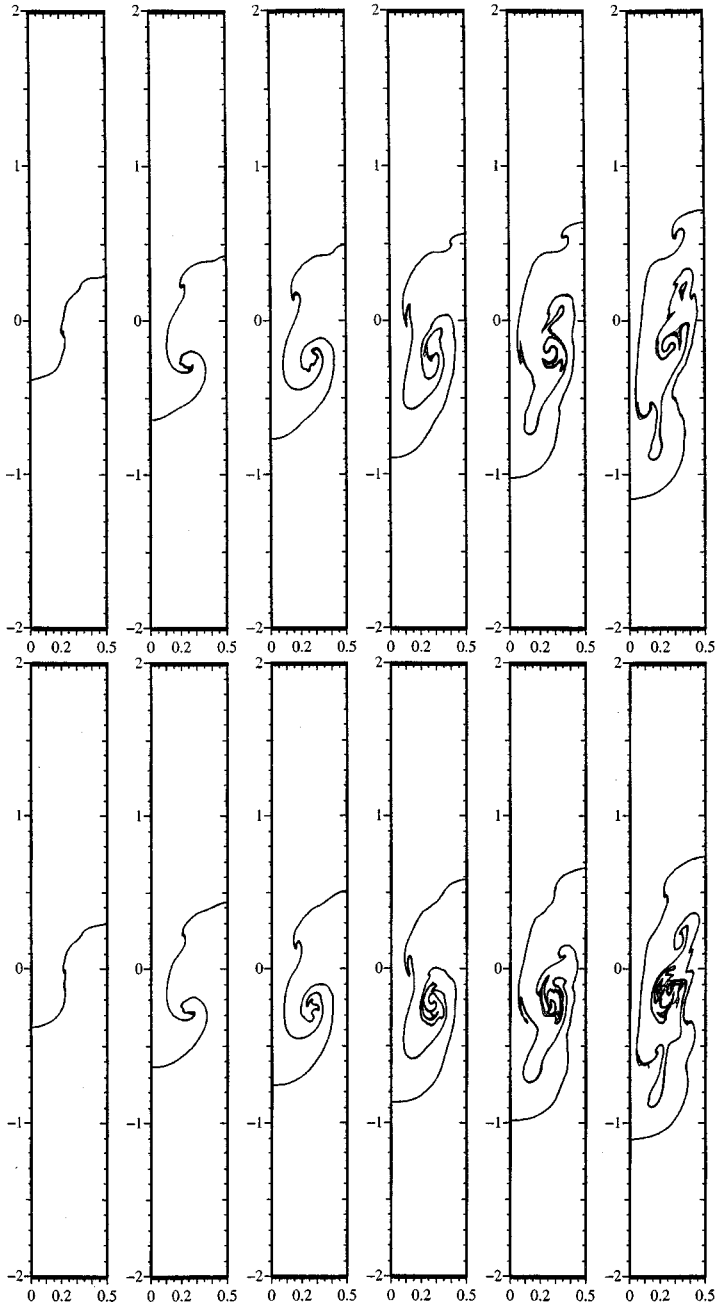

FIG. 3. Re = 5000; density ratio 3. The grid is composed of 30,189 $\mathbb{P}_2$ nodes (top) and 49,577 $\mathbb{P}_2$ nodes (bottom). The initial amplitude is 10% of the wavelength. The interface is shown at times 1, 1.5, 1.75, 2, 2.25, and 2.5 (density contours $1.4 \leq \rho \leq 1.6$).

[15, Fig. 4], especially in the early stage. Note however that the roll-up of the the main vortex in the present calculation does not develop since the singularity at the center of the vortex is removed by viscous dissipation.

All these results indicate that an accurate and detailed prediction of such a flow for $t \geq 1.5$ and $\mathrm{Re} \geq 5000$ is a difficult task, at least for the proposed projection method. In any case,

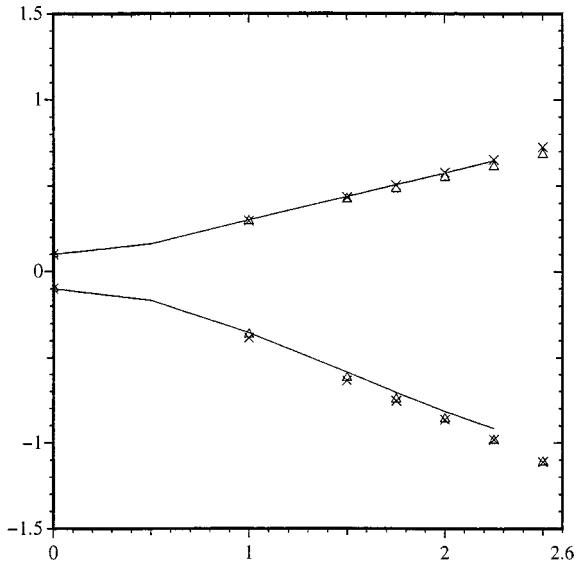

FIG. 4. Position of rising and falling bubbles versus time. Solid line: inviscid computations from Tryggvason [15]. Symbols denote results by projection method: △: Re = 1000; ×: Re = 5000.

note that our Re = 5000 solution is so different from the inviscid one reported in [15] that we face the question of whether the infinite Reynolds limit of the viscous solution should be equal to the inviscid solution. In this respect, we recall that "Birkhoff has speculated that the initial-value problem [for inviscid stratified flows] might be ill-posed [as a consequence of the fact that] the growth rate of an infinitely small unstable wave is proportional to the square root of its wave number," as reported by Tryggvason [15]. As a result, the authors' knowledge seems to leave the question of the existence of a smooth inviscid solution for large times open.

6.3. *A High Atwood Number Problem*

To complete the set of comparisons, we have run the test case described in [1]. The geometry is the same as in the previous test case. The density ratio is 7, so At = 0.75 (corresponding to the value 0.875 using the definition of the Atwood number in [1]). The perturbation of the interface is $\eta(x) = -0.01d\cos(2\pi x/d)$ and the transition between the two fluids is regularized by means of the following law:

$$\frac{\rho_0(x, y)}{\rho_{\min}} = 4 + 3\tanh\left(\frac{y - \eta(x)}{0.01d}\right).$$

The location of the interface at times 1, 1.5, 2, 2.5, 3, 3.5, 3.75, 4, 4.25 is shown in Fig. 5 on two grids composed of 30,189 and 49,577 $\mathbb{P}_2$ nodes, respectively. From the qualitative point of view, the two solutions exhibits the same structures. The main difference consists in a small time delay in the roll-up of the rising bubble that prompts different interactions between the two vortices at large times. On the coarse mesh, there is a strong interaction, whereas on the fine grid the two vortices develop almost independently. Note that in both cases the two vortices seem to have self-similar behaviors in the early stages of their development. By inspecting the two solutions at time 1.5, we see that more Fourier modes

FIG. 5. Re = 1000; density ratio 7. The grid is composed of 30,189 $\mathbb{P}_2$ nodes (top) and 49,577 $\mathbb{P}_2$ nodes (bottom). The initial amplitude is 1% of the wavelength. The interface is shown at times 1, 1.5, 2, 2.5, 3, 3.5, 3.75, 4, and 4.25 (density contours $2 \leq \rho \leq 4$.).

are active on the fine mesh than on the coarse one. This can be understood in the light of the aforementioned Birkhoff's conjecture. In fact, in the early stage of the evolution the viscous effects are negligible and small scale perturbations are produced from the perturbed initial data by nonlinear interactions. The finer the mesh, the larger the spectrum of available unstable modes. By virtue of the linear stability argument of Birkhoff, the smaller the scale of the unstable modes the higher their growth rate. Because our numerical scheme has negligible artificial damping, small unstable modes are rapidly amplified. As a result, at $t = 1.5$ we distinguish four structures on the interface for the coarse grid whereas five are present for the fine mesh. Note that, as observed by Tryggvason [15, p. 268], some

of these vortices merge into one big vortex. Actually, three vortices out of four merge on the coarse mesh whereas four out of five merge on the fine grid. This mechanism may explain the anticipated formation of the secondary vortex on the coarse mesh. Note also that this argument can also explain the delay in the formation of the secondary vortex that we observed on the previous test case when comparing the coarse and the fine solution at $\mathrm{Re} = 5000$.

We have chosen this test with the hope of reproducing the results of [1]. We must admit that our solution and that of [1] are quite different. The main reason for this difference is that in our simulation small unstable modes develop at the early stage of the time evolution whereas these modes seem absent in the computation reported in [1]. It is likely that the completely different treatments of the nonlinear inertial terms by the proposed unconditionally stable finite element method and by the referred Godunov-based approach are at the origin of the discrepancy. The clarification of this issue is left for future investigations.

7. CONCLUSIONS

In this work, we have extended the incremental projection method to the case of incompressible viscous flows with nonuniform density. We have recast the momentum equation in a new manner to guarantee that the spatial discretization errors associated with the satisfaction of the mass conservation cannot affect the balance of the kinetic energy of the fluid. The proposed form allows for developing unconditionally stable projection schemes with the condition of incompressibility replaced by an elliptic equation for pressure, with a variable coefficient depending on the density. A second-order accurate projection scheme has been obtained which is based on performing two projections per time step and using a three level BDF scheme for the time integration of the mass conservation and momentum equations. The spatial approximation is performed by means of Lagrangian finite elements with $\mathbb{P}_2$ interpolation for density and velocity and $\mathbb{P}_1$ interpolation for pressure.

To verify the correctness of the method, it has been applied to two test cases previously considered in the literature. These problems consist in simulating the evolution of the Rayleigh–Taylor instability of the interface between fluids of different densities. While for a low density ratio (Atwood number $= 0.5$) the results of the new projection method in the range $\mathrm{Re} \approx 1000$ are in agreement with the inviscid computations [15] in the early stages of vortex formation and roll-up, for a high density ratio (Atwood number $= 0.75$) substantial differences are found with the results provided by the finite difference projection method of Bell and Marcus [1]. The analysis of spatial convergence conducted for the test problem at the higher Atwood number indicates that the proposed method is accurate and reliable enough for considering the computed solutions worth of attention for further comparisons.

ACKNOWLEDGMENT

The authors are grateful to Ivan Delbende for discussions and remarks that greatly improved the content of this paper.

REFERENCES

1. J. B. Bell and D. L. Marcus, *J. Comput. Phys.* **101**, 334 (1992).
2. A. J. Chorin, *Math. Comp.* **22**, 745 (1968).
3. A. J. Chorin, *Math. Comp.* **23**, 341 (1969).

4. J.-L. Guermond, *C. R. Acad. Sc. Paris Sér. I* **319**, 887 (1994).
5. J.-L. Guermond, *Modél. Math. Anal. Numér.* **33**, 169 (1999).
6. J.-L. Guermond, *Modél. Math. Anal. Numér.* **33**, 1293 (1999).
7. J.-L. Guermond and L. Quartapelle, *J. Comput. Phys.* **132**, 12 (1997).
8. J.-L. Guermond and L. Quartapelle, *in* "Navier–Stokes Equations: Theory and numerical methods," edited by R. Salvi (Longman, Harlow/New York and Pitman, London, 1998), Vol. 388, pp. 277 to 288.
9. J.-L. Guermond and L. Quartapelle, *Numer. Math.* **80**, 207 (1998).
10. P.-L. Lions, "Mathematical Topics in Fluid Mechanics. Volume 1. Incompressible Models" (Clarendon, Oxford, 1996).
11. R. Rannacher, Lecture Notes in Mathematics (Springer-Verlag, Berlin, 1992), Vol. 1530, p. 167.
12. Shen, Jie, *Math. Comput.* **65**, 1039 (1996).
13. R. Temam, "Navier–Stokes Equations," Studies in Mathematics and Its Applications 2 (North-Holland, Amsterdam, 1977), Vol. 2.
14. R. Temam, *Arch. Rat. Mech. Anal.* **33**, 377 (1969).
15. G. Tryggvason, *J. Comput. Phys.* **75**, 253 (1988).